Estuarine, Coastal and Shelf Science 265 (2022) 107694

Contents lists available at ScienceDirect

Estuarine, Coastal and Shelf Science

journal homepage: www.elsevier.com/locate/ecss

Numerical investigation of the effects of distributary bathymetry and roughness on tidal hydrodynamics of Wax Lake region under calm conditions

Hassan Shafiei [a], Antoine Soloy [b,*], Imen Turki [b], Marc Simard [c], Nicolas Lecoq [b], Benoit Laignel [b]

[a] Laboratory of Geophysical and Industrial Flows (LEGI), University of Grenoble Alpes, G-INP, CNRS, 38000, Grenoble, France
[b] Normandie University, UNIROUEN, UNICAEN, CNRS, M2C, Morphodynamique Continentale et Côtière, 76000, Rouen, France
[c] Jet Propulsion Laboratory, California Institute of Technology, Pasadena, CA, USA

ARTICLE INFO

Keywords:
Hydrodynamic modeling
Floodplains
Wax lake region
Delf3D-FLOW
SWOT

ABSTRACT

In this paper, we investigate the effects of the bathymetry of the floodplain distributaries using a 2-dimensional hydrodynamic model of the Wax Lake Outlet (WLO), delta and floodplain (Louisiana, USA), using Delft3D. Modelling the tidal-fluvial interaction of this region is challenging because of its complex network of low-lying floodplain distributaries and vegetation coverage. This investigation addresses this interaction by generating the evolution of the flood-map that is used in the calibration and validation phase of the Surface Water and Ocean Topography (SWOT) mission. Accordingly, the model is set up for one week of calm conditions from October 14th to 20th in 2016. Boundary conditions applied at the edges of the 36×23 km^2 domain include the offshore water level with tidal oscillations, the upstream volumetric river discharge rate and wind time-series (applied spatially uniformly). The topo-bathymetry of the domain is a product of the Pre-Delta-X mission; however, it has considerable uncertainties to represent the small distributaries, especially in the forested section of the region. This paper tackles this uncertainty by parametrically enhancing and calibrating the primary Digital Terrain Model (DTM). The performance of the model is assessed using the water-level time series measured by the stations spread throughout the floodplain, delta and main river. The results show that the morphology of the distributaries play a major role in the hydrodynamic of Wax Lake region under calm conditions. The hydrodynamic of the WLO and floodplain is considerably affected by the discharge capacity of the distributaries (changed by editing their width and depth) due to change of the balance between roughness and topographic convergence. In WLO, higher discharge capacity leads to higher overall roughness friction force, thereby dampening the amplitude of the water-level signal and vice versa. On the other hand, increasing the bottom roughness of the WLO increases the water level in the floodplain, with more considerable effect in the low tides. The calibrated model well matches the measurements along the Wax Lake Outlet. However, the main discrepancies are in the stations further away from the WLO. The tests conducted in this research suggest that the excessive roughness due to uneven bed along the distributaries and vegetation are, respectively, the potentially-responsible parameters for the remaining discrepancies in low- and high-tide periods.

1. Introduction

Coastal wetlands act as a major reserve of biodiversity (Sievers et al., 2019; Xie et al., 2019), a highly productive carbon sink (Mcleod et al., 2011; Shields et al., 2017), a water quality and nutrient cycle regulator (Megonigal and Neubauer, 2019; Rivera-Monroy et al., 2011), and a protective barrier against storms and tsunamis (Barbier et al., 2013; Kathiresan and Rajendran, 2005). These regions are subject to a series of complex and interacting natural processes responsible for weathering, marine erosion and flooding hazards (Nicholls et al., 2007). The impacts of these processes are usually site-dependent, changing with bathymetric and energy conditions.

The non-linear interactions between these forcings increase the complexity of hydro- and morphological dynamics of coastal areas; for example (Jay et al., 2015), studied the tidal-fluvial water level in a river and concluded that the relationship is non-linear and non-stationary.

* Corresponding author.
E-mail address: antoine.soloy@univ-rouen.fr (A. Soloy).

https://doi.org/10.1016/j.ecss.2021.107694
Received 7 January 2021; Received in revised form 17 November 2021; Accepted 2 December 2021
Available online 14 December 2021

Furthermore, the non-linear effects of bathymetry (e.g. channel cross-section and bottom profile), roughness and vegetation on hydrodynamic (e.g., turbulence mixing, dissipation, velocity and water level) make modeling of these regions challenging (Gross and Werner, 1994; Marsooli et al., 2016; Osorio-Cano et al., 2019). In the context of climate change and sea-level rise, predicting the flow of water in tidal rivers and their floodplain is critical. Buschman et al. (2010) developed a model to predict the flow division in a tidal junction, showing that the inlet stokes transport is not necessarily equal to the Eulerian return transport and depends on many factors such as channel depth, width, length, roughness and asymmetry (Sassi et al., 2011). continued the work of (Buschman et al., 2010) and concluded that the neighboring channels affect each other's hydrodynamic. Further (Hoitink and Jay, 2016), reviewed the methods for analyzing water level and inundation extent in various tidal rivers. Moreover (Leonardi et al., 2015), studied the river-tide interaction in a delta and concluded that regardless of the strength of the fluvial discharge, tide strongly affects the hydrodynamic of the delta.

This complexity increases especially in vegetated environments (Zhang et al., 2018). Indeed, the presence of vegetation has a significant impact on coastal wetland hydrodynamics by obstructing the water flow (Temmerman et al., 2007). Furthermore, it changes the bottom erosion resistance, turbulence mixing, flow resistance, wetted area, and inundation (Al-Asadi and Duan, 2017; Baptist et al., 2007; Horstman et al., 2014, 2018; Hu et al., 2015; Jay et al., 2016; Nardin et al., 2016).

The Mississippi River Delta region is an ideal study site to understand the multi-scale evolution of coastal wetlands with a long-term and dense in-situ instrument network. In particular, the evolution of the Wax Lake Delta (WLD, western region of the Mississippi River Delta floodplain) can be tracked from its initiation because it was naturally formed after the construction of the Wax Lake Outlet (WLO) by the United States Army Corps of Engineers (USACE) in 1942 (Hanegan, 2011). Extensive research has been conducted in the WLD region to understand its hydrodynamics (Hanegan, 2011; F Xing et al., 2013; Zhang, 2015), morphodynamics (Edmonds and Slingerland, 2007; Parker and Sequeiros, 2006; Xing et al., 2017), and biological and ecological evolution (Carle, 2013; Olliver and Edmonds, 2017; Shaffer and Sassert, 2018). However, the previous models focused on the WLO and Wax Lake delta at its mouth (Christensen, 2017; Hanegan, 2011; Xing et al., 2017; Zhang, 2015); they generally neglected the dynamics of the intertidal wetlands on either sides of the WLO. One of the main challenges is the lack of detailed Digital Terrain Model (DTM) which is an essential requirement in hydrodynamic modeling of plain regions like Wax Lake floodplain. In these types of environments, small topographic variations influence the water storage and flow velocity considerably more than those in the regions with steep slopes (Jung and Jasinski, 2015).

In the framework of the Surface Water and Ocean Topography (SWOT) mission, the results of this study will be used in the validation and calibration phase by providing the map of the water-surface evolution in one of the sites being studied in the SWOT mission (i.e., Wax Lake region); the particular focus is on the hydrodynamics of the WLO floodplain. One of the objectives of the SWOT mission is to provide surface-water topography measurements along rivers, lakes, streams, and wetlands and over the ocean surface using swath altimetry with the orbit repeat period of about 21 days. The spatial resolution of SWOT products would be 1 km and 100 m for the ocean and land water respectively. Furthermore, the elevation accuracy would be about 3 cm for ocean and 10 cm for land water surface (Durand et al., 2010; Neeck et al., 2012; Marc Simard et al., 2019). The results of the current investigation would be utilized as an input into the SWOT simulator (e.g., Gaultier et al., 2010; Gomez-Navarro et al., 2018). Therefore, the spatial and temporal resolutions of the current modeling are chosen accordingly.

Within the context of SWOT, this paper presents the use of a hydrodynamic models for SWOT calibration and validation in a flat intertidal area containing river, delta and a complex network of floodplain distributaries. An approach is also introduced to calibrate the bathymetry of the vegetated floodplain which initially may not have accurate digital elevation models. Knowledge of water-surface elevation summarizes information about the different acting physical forcing, as well as their interaction with one another and with the local geomorphology. With this in mind, this study's goal is to address the following questions:

- Which and how do some local environmental settings influence the water level variability?
- What combination of geomorphological parameters such as the drag coefficient and channel geometry allow the best reconstruction of the Wax Lake region's hydrodynamics for calm conditions?
- How is the tidal oscillatory signal transformed along its propagation through the distributary channel network?

In Section 2, we introduce the study site. In Section 3, the Delft3D model and its configuration are summarized, with a description of the processing methodologies applied to the hydrodynamical and morphological data. The model results are discussed in Section 4 with a particular attention given to having the best result following a systematic procedure rather than a manual one (so that it can be applied to other areas and scales). The respective results of the bathymetry calibration will also be discussed in this section. Furthermore, some suggestions are explained to further improve the model. Conclusive remarks will be presented in the fifth and final Section.

2. Study site

The WLO is an artificial canal connecting the Wax Lake and the Gulf of Mexico that was built by the USACE in 1942 in order to divert 30% of the flow from the Atchafalaya River to the sea and prevent flooding in the surrounding cities (Davidson et al., 1988). The construction of the canal delivered 34 Megatons of sediment per year (Kim et al., 2009), naturally forming the Wax Lake Delta that pro-graded 8 km toward the sea in 64 years. The evolution of this delta is not controlled, providing an ideal large scale experiment to study river delta formation (Christensen, 2017; Hanegan, 2011; Xing et al., 2017; Zhang, 2015). Along with the Atchafalaya River Delta, the Wax Lake Delta is one of the only places in the Mississippi River Delta region subject to prograding, while the rest of the coast is receding (Hiatt, 2013). The measured discharge at the Calumet station located 18 km north of Wax Lake delta (shown with grey circle in Fig. 1a) has an average flow of 2500 m^3/s with annual floods exceeding 5000 m^3/s (Hiatt, 2013; Rouse et al., 1978). Furthermore, the station (shown with white circle in Fig. 1a) at the southeastern corner of the domain is where the tidal inlet conditions were measured; the yellow and orange circles represent the observation point used for evaluations of the results. Wax Lake outlet's depth is about 25 m upstream, 20 m downstream and 5 m in the delta fan (Fig. 1 b and c).

3. Methodological approach

The present study was realized using the Delft3D two-dimensional (depth-averaged) model fed with data provided by NASA/Jet Propulsion Laboratory (JPL), the United States Geological Survey (USGS), the National Oceanic and Atmospheric Administration (NOAA) and Google.[1] In this section, these data and tools will be described.

3.1. Delft3D

The Delft3D is a package of integrated modules developed by Deltares to simulate flow hydrodynamics, sediment transport, morphological processes, and water quality aspects in the coastal, river, and

[1] https://mt1.google.com/vt/lyrs = r&x = {x}&y = {y}&z = {z}.

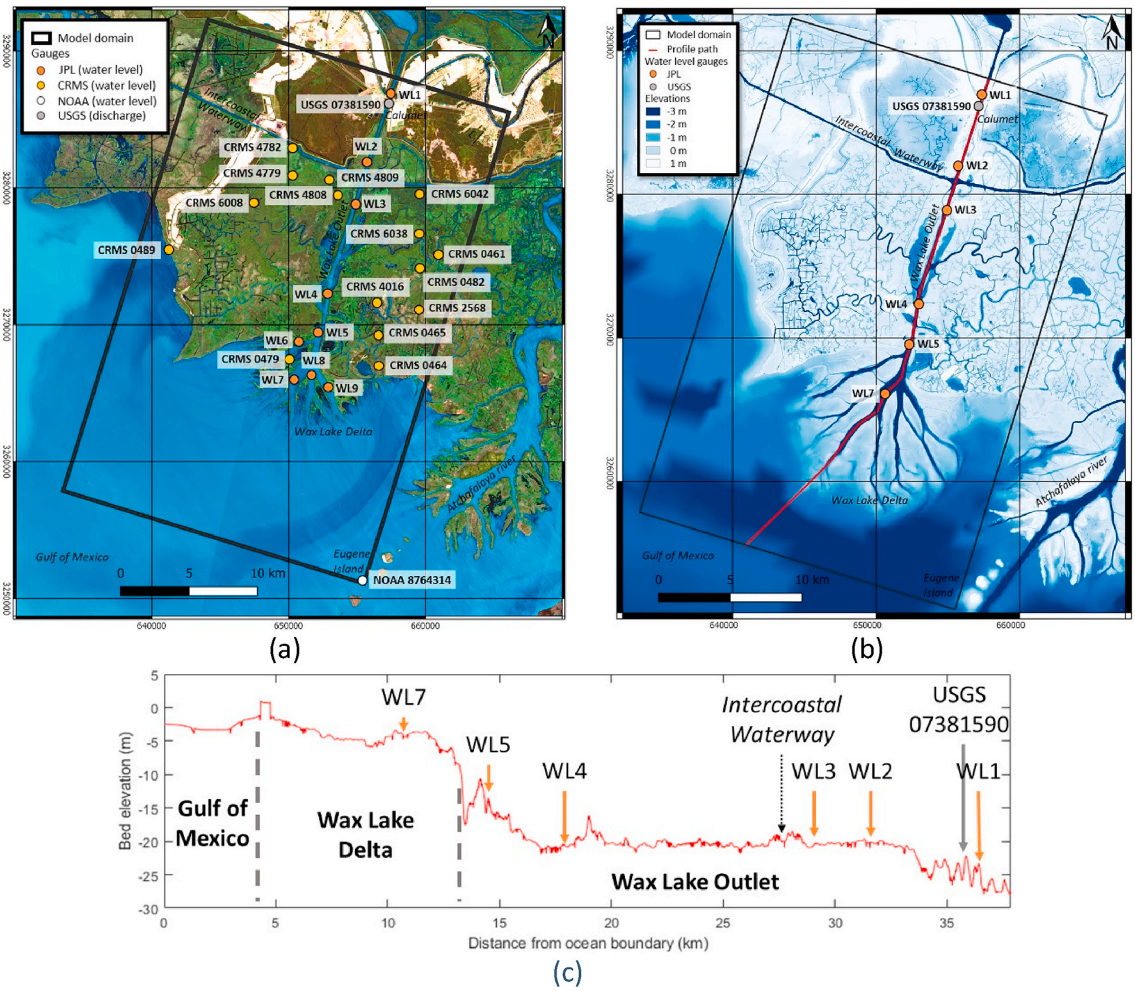

Fig. 1. (a) The study area and the location of the measurement stations used for model input and validation of the results, (b) The calibrated DTM of the study area and (c) the bottom profile of the WLO and the main pass of the Wax Lake Delta. (NAVD88).

estuarine areas (Roelvink and Van Banning, 1995). The hydrodynamic module is named as Delft3D-FLOW and solves the two-dimensional (depth-averaged) and three-dimensional unsteady shallow-water equations (Lesser et al., 2004). The two-dimensional depth-averaged momentum equations are obtained by integrating the three-dimensional hydrostatic shallow-water equations from the bottom to the free surface (in the 3D model, the third dimension,i.e. depth, is scaled from -1 to 0 (Gerritsen et al., 2008; Stelling and Van Kester, 1994)).

Delft3D-FLOW wetting-drying algorithm is effective and accurate for the flows with large gradients of water level. It obtains the water level in the center of each cell using the computed water depth at the cell nodes. Then, it calculates the total water depth at each velocity point. If the value is lower than the half of the user-defined depth threshold, the water-depth is set to zero at that point. Finally, if all four velocity points in a cell are zero, the cell is considered as dry (i.e., it becomes a closed boundary). The cell will be considered wet again if the total water depth becomes higher than that threshold (Deltares, 2014).

3.2. Model description

In the present model setup, tide-induced water elevation, river-discharge flow rate, and wind velocity were used in order to simulate the hydrodynamics of Wax Lake Delta and surrounding intertidal area. The desired simulation period ranges from October 14th, 2016 at 00:00:00 UTC to October 20th, 2016 at 00:00:00 UTC. However, to give the simulation enough time so that the inlet tide reaches the northern stations, it was necessary to start the computation earlier in order to ensure the model converges to a steady state in the distributary channels in the wetlands. For this purpose, the simulation was set to start on October 2nd, 2016.

3.2.1. DTM data and processing

The calibrated Digital Terrain Model (DTM) used in this research is presented in Fig. 1b. The original version was produced by the Pre-Delta-X mission (M. W. Denbina et al., 2020). It is a 10-m-resolution DTM derived from merging of four different data sources, each with different horizontal and vertical accuracies. One of the main data source is Shaw et al. (2016), with root-mean-square error of 0.1 m (by comparing the bathymetric surfaces to surveyed lines). More information about the uncertainty of the sounder measurements they used as well as the effect of the interpolation they performed is explained in section 7.2 of (Whaling and Shaw, 2020). The other three data sources include the land topography from the USGS National Elevation Dataset (NED) (Gesch et al., 2002), with a global-scale RMSE of 2.4 m; a bathymetry of the bay by Xing et al. (2017); and sonar measurements collected during Pre-Delta-X campaigns in May 2015 and November 2016 (M. W. Denbina et al., 2020).

However, the primary bathymetry was not sufficiently accurate to allow for a realistic flow of water especially into the forested floodplain. This is in part due to limited bathymetric measurements in areas covered by vegetation. In this investigation, a calibration approach (with the potential applicability to a more extended DTM of the region covering the Atchafalaya river and floodplain) is suggested to modify the original DTM. For achieving this goal, Google-map water mask (Google, n.d.) proved to be detailed enough to be used as a raster selector in modifying the distributary network of the primary DTM. The original pixel size of the water mask is 60×60 cm^2, which is upscaled to 10×10 m^2 to match the primary DTM to be modified. This Google-Maps water mask (Google, n.d.) is then used to improve the channel network configuration, depth, and width across the floodplain. The modification procedure includes (1) selecting the pixels that need to be modified and (2) digging the selected pixels adequately. Using the QGIS raster calculator,[2] the initial DTM is used to identify the floodplain (by choosing $-3.35 <$depth<2, in meters) from the Wax Lake Outlet, Wax Lake Delta and Gulf of Mexico. Furthermore, the water-mask raster values (between the values corresponding to water and dry land) are used to control the connectivity of the distributaries in the floodplain (using the QGIS raster calculator). However, increasing the connectivity makes the distributaries wider (since the values of the pixels on the edges of the distributaries and those increasing the connectivity are almost the same). Thus, the connectivity must be increased carefully so that the width of the distributaries is not exaggerated. In this study, two connectivity configurations (see Fig. 2) are examined. Hereafter, the resultant modified DTM using these two configurations are distinguished by using either 'wide' or 'narrow' in their respective names. In the next step, the depth of the selected pixels is increased uniformly by subtracting a constant value from their terrain elevation using the primary DTM. However, since no data are available regarding the actual depths of these channels, different digging values are tested, and their respective modelled water levels are compared. Here, the results of the cases in which the selected pixels are dug by 1, 1.5, 2 and 2.5 m are presented and discussed (note that the values out of this range result higher water-level deviations from the measurements). Hereafter in this paper, they are distinguished by their respective digging values (i.e., either 1 m, 1.5 m, 2 m or 2.5 m) in their names (note that the grid is kept the same as will be explained in Section 3.4). More details about the effects of these modifications on the hydrodynamics are presented in the section 4.1.

Seven versions of the modified DTMs are presented in this study (hereinafter named as narrow 1 m, narrow 1.5 m, narrow 2 m, narrow 2.5 m, wide 1 m, wide 1.5 m and wide 2.5 m). Fig. 2 compares some of these DTMs by illustrating the depths and widths of a distributary channels in the northwestern forested part of the Wax Lake wetlands. Part (a) shows a selected section of the primary DTM as well as the distributary channel whose cross-section is illustrated in part (b) of Fig. 2. And parts (c)–(f) compare the network of the distributary channels in the north-western side of WLO in these modified DTM versions. Fig. 2c shows the DTM modified by digging the distributary channels by 1.5 m (in this paper, it is named as narrow 1.5-m depth DTM correction). The other parts (d), (e) and (f) present the distributaries created using a wider range of pixels which lead to more channel connectivity and wider channels (they will be named as 'wide' followed by their depth correction value).

Note that the resolution of the DTM is higher than that of the model; therefore, *Grid Cell Averaging* (in Delft3D) is used to generate the bathymetry of the model (i.e., *.dep file). Therefore, to test the effects of the flattened bed of the distributaries, the Delft3D depth file (*.dep), rather than DTM, is edited. The bed of the distributaries is flattened by simply replacing all the computational cells within a certain depth range by a constant value.

3.2.2. Input parameters

Water level and wind data (Fig. 3) were measured at 3-min interval at NOAA's Eugene Island station 8764314. The vertical reference used for the water levels is the North American Vertical Datum of 1988 (NAVD88). We can observe that the river discharge is almost constant in comparison to other periods, and the average water level and wind speed are 0.52 m and 1.82 m/s respectively. Furthermore, the WLO flow rate was measured every 3 min at USGS′ Calumet station 07381590.

3.3. Evaluation data

In-situ measurements of water level from the USGS Coastwide Reference Monitoring System (CRMS) stations (Steyer, 2010) and nine additional stations installed specifically for the AirSWOT campaign (M. Denbina et al., 2019) were used for evaluating the model. The measurements of the CRMS stations (Fig. 1a) are according to vertical reference NAVD88. Moreover, the nine temporary stations recorded water level using pressure transducers (Solinst levelogger®) between October 13th and 20th of 2016 (vertical datum NAVD88) to validate AirSWOT measurements (M Simard et al., 2020), shown in Fig. 1a as WL1-WL9. The above-mentioned stations are located throughout the numerical domain: WL1 to WL5 are along the Wax Lake Outlet, and WL6 to WL9 as well as CRMS0479 are in the Wax Lake delta. Some of stations are near the eastern coast of the domain (i.e., CRMS0464 and CRMS0465) and some are in the eastern marshland (i.e., CRMS2568 and CRMS4016). There is one station on the coast near the western boundary of the domain (i.e., CRMS0489) and one along the bank of intercoastal water way (i.e., CRMS4782). The rest of the stations are on the western (i.e., CRMS6008, CRMS4779, CRMS4808, and CRMS4809) and eastern (i.e., CRMS 6042, CRMS6038, and CRMS0461) forested floodplain respectively.

3.4. Numerical model configuration

The modified DTMs explained in section 3.2.1 (with the resolution of 10×10 m^2) are interpolated into a regular uniform grid with the resolutions of 46×45 m^2 (Fig. 4, with a 0.25-min time-step). Interestingly, using a finer mesh increases the computational cost while the results (especially during low tide) do not improve considerably. This may be related to the high uncertainty of the DTM in representing the bottom profile of the distributaries, as explained by (Jung and Jasinski, 2015). As also will be explained later in Section 4.2, flattening the bed of the distributaries (i.e., replacing the depth values along the distributaries with a constant depth) improved the results during the low tide periods, emphasizing on the need to revise the bottom depth profiles along the distributaries especially in the forested region of the floodplain. However, finding an approach to revise the DTM to represent a more precise bottom profile of the distributaries remains a challenge. As explained in Section 3.2.1, the constant-depth distributaries tested in the current model are obtained by revising the **.dep* file in the Delft3D model rather than the DTM file.

In this paper, we evaluate the model at the resolution accepted for the SWOT simulator, i.e. 50×50 m^2. Furthermore, especially at the stations experiencing lower water depths, the threshold for drying/wetting procedure (explained in Section 3.1) becomes important. In this model, *Threshold depth* $= 0.01$ m was found to be a suitable choice.

In the first stage, we use uniform Manning's coefficients of $n = 0.018$, 0.02, 0.022, and 0.025 s/m$^{1/3}$ for all the modified DTMs, choose most suitable value for Manning's coefficient, then select the best case (explained briefly in Section 4.1). Afterwards, we use non-uniform Manning's coefficient for the best case chosen in the previous stage. Two approaches are tested to apply non-uniform Manning's coefficient: (1) applying different values of Manning's coefficient for each region using *Polygon* (in Delft3D) in Delft3D-QUCKIN (dividing the domain into five sections of main river, delta, eastern floodplain, western floodplain and Gulf of Mexico) (2) using the depth of the cells as a criterion to choose their respective allocated Manning's coefficient. This is done simply by replacing the depth values (in **.dep* file in Delft3D) within a certain range by the corresponding Manning's coefficient, then use the file as a roughness input file (**.rgh* file in Delft3D). In this study, the focus is on approaching an automatic procedure with the least manual

[2] http://qgis.osgeo.org/.

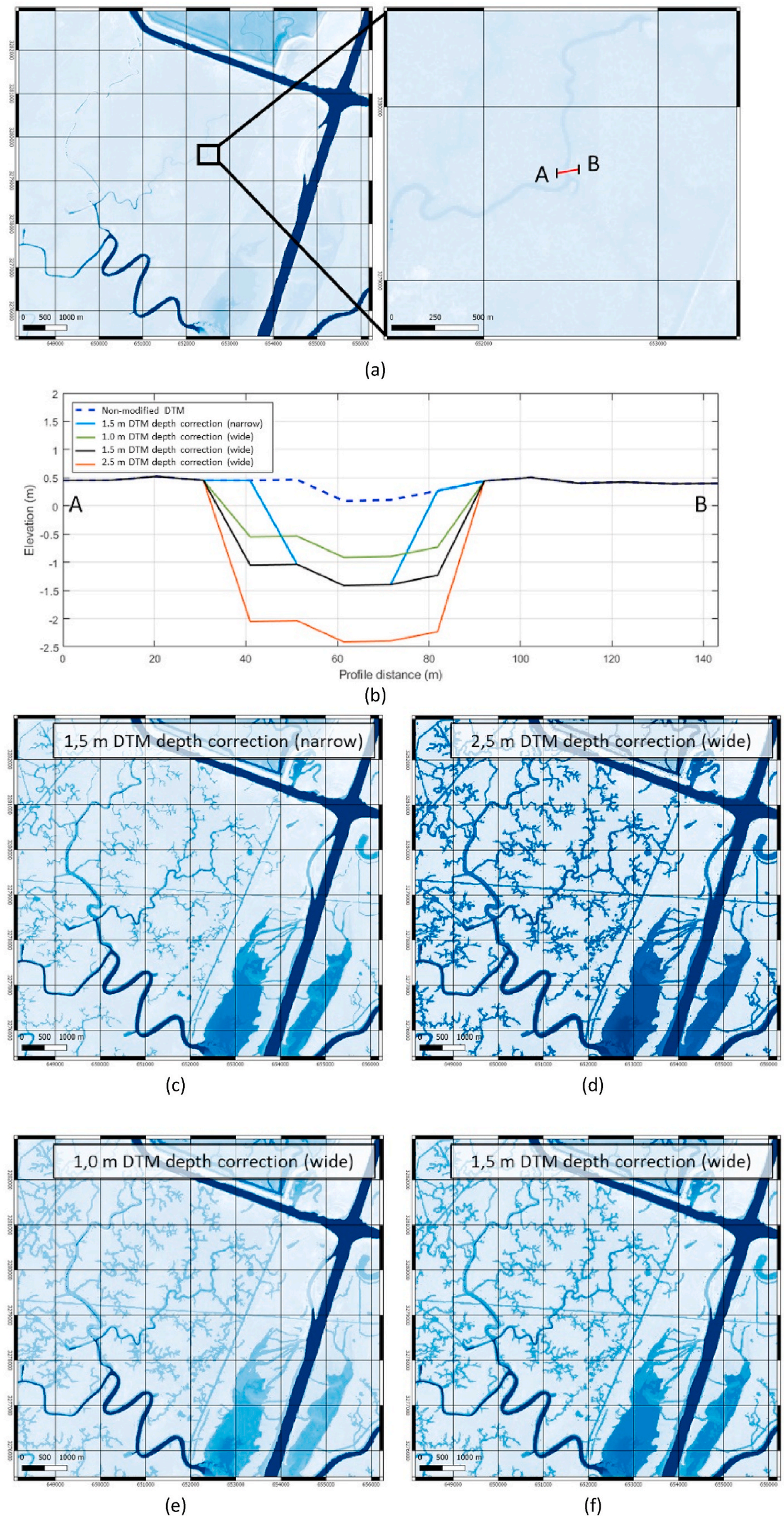

Fig. 2. Illustration of the northwestern floodplain section of some of the modified DTMs (a): primary DTM, (b): bottom cross-sectional changes of an arbitrary distributary channel shown in part (a), (c)–(f): the top view of the same section as part (a) corresponding to four selected versions of DTM modification.

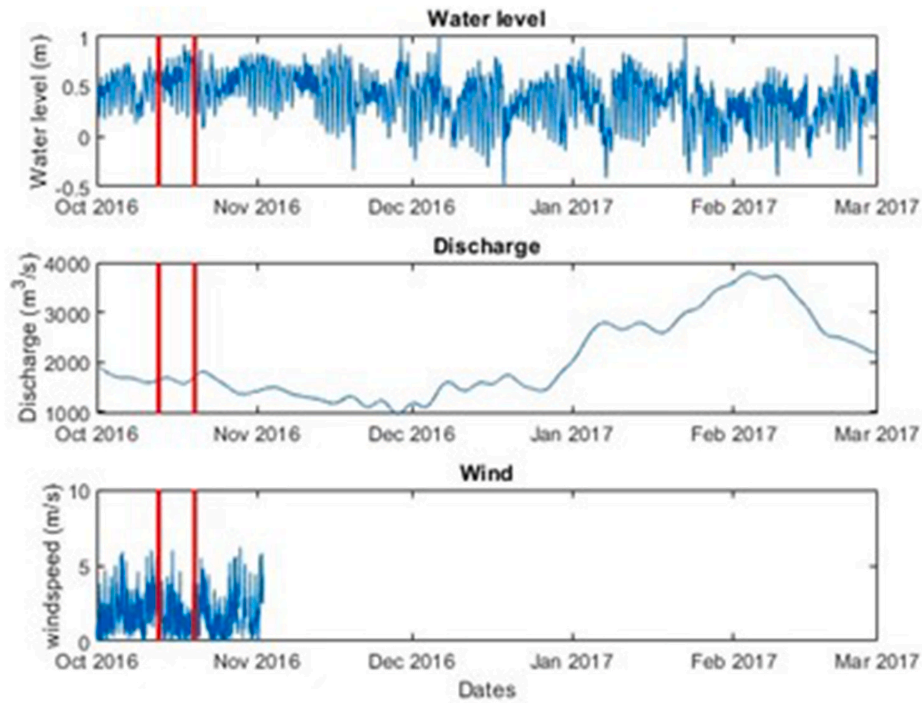

Fig. 3. Time series of water level, river discharge, and wind speed used within the model's time range (vertical red line). (For interpretation of the references to color in this figure legend, the reader is referred to the Web version of this article.)

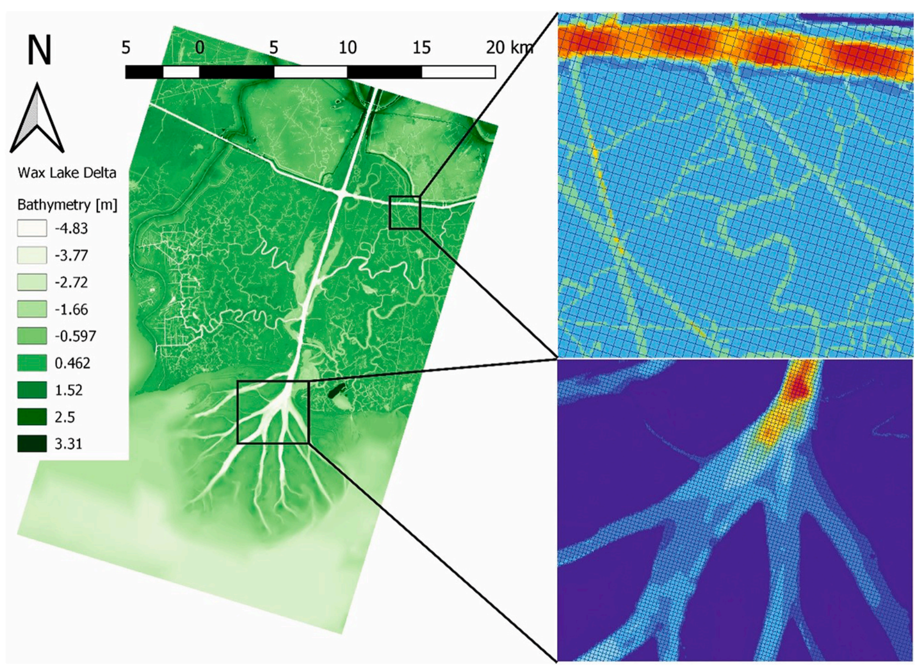

Fig. 4. Illustration of the uniform structured grid (the right-hand-side of the figure, with resolution of 46 × 45 m^2) used in the simulations presented in this paper.

settings involved so that it can also be applied in future studies. Furthermore, each station in the domain behaves differently (i.e., some need to be drained more in the low tides, some need to receive less water mass, some have longer inundation periods, etc.) which makes predicting the appropriate Manning's coefficient for each region difficult, especially considering that some of the adjacent stations are interconnected through multiple distributaries). It was also observed that due to small depth variation across the flood plain, there were no significant differences between the results of the two approaches (not presented here); the second approach is preferred due to its simplicity and smoother roughness transition to the adjacent cells.

Four types of boundary conditions (BCs) are used in the domain. The tides enter the domain perpendicularly to the southern boundary using water-level time-series, and the river discharge is inputted as discharge time-series from the intersection line of the WLO and the northern boundary. The other parts of the northern boundary are enclosed by levees and thus are closed boundaries in the model. The western boundary is completely isolated behind levees, outside of the domain of interest. On the other hand, the eastern boundary is within the floodplain. Comparing the results of stations nearby this boundary, we found that a wall BC produced more realistic results than the Neumann BC. The Neumann BC produced excessive inlet of water mass when the cells along the eastern boundary were dried after each high-tide period (for future studies, we recommend to include the Atchafalaya river and floodplain also). For the sea section of the eastern and western boundaries, considering the fact that the tides are imposed perpendicular to the southern boundary and neglecting the alongshore water-level gradient, the Neumann BC was found suitable (Deltares, 2014). It should be noted that the boundary conditions at the inlet and outlet of the intercoastal waterway (ICWW) are considered to be wall BC, meaning that its flow within the domain is neglected. As explained by Hanegan (2011), the reasons behind this assumption are, firstly, the flow in this channel is relatively small in comparison to the one in Wax Lake Outlet. Secondly, the average flow exchange between the two channels is negligible (i.e., the flow rate entering the domain through ICWW is approximately equal to the one exiting through it on the other side of the domain), making its effects on the hydrodynamic of the region small.

Furthermore, to test the effects of vegetation and support the assumption of neglecting them in this work, Baptist 2 formulation (Baptist et al., 2007) is used in this Delft3D model (the results are not presented in this paper due to the negligible effect in improving the results). This formulation is classified as the vegetation area class of tranchytope in which a vegetation-induced flow resistance term is added to the momentum equation. This gives the advantage of separating the vegetation effects from the bed roughness. In this model, first, the computational cells to include vegetation are selected using the Sentinel-2 radar data (Thomas et al., 2019) representing three vegetation coverage types of forest, marsh and bare. Then, for each cell, rough values for the density of forest and marsh are calculated using the same Sentinel-2 radar data. Finally, some sensitivity testes are performed to examine the effects of vegetation input parameters (e.g., vegetation height, density and drag coefficient); however, none of the tests improved the results.

4. Results and discussions

4.1. Bathymetry calibration

The most suitable DTM is chosen following a calibration approach by comparing their respective modelled water level with the observations (Fig. 5). The model outputs are compared to the observed dynamics in the Wax Lake Outlet's main channel and delta using the data recorded during the JPL field campaign of November 2016 (M Simard et al., 2020) and in the intertidal floodplain using the CRMS data (Steyer, 2010). While the original DTM, left some of the CRMS stations located in the floodplain dry (e.g., CRMS6042), even after 18 days of simulation (i.e., October 02, 2016–October 20, 2016), it was found that modifying the DTM solved the problem of the dry stations. This calibration approach gives a good insight on how the bathymetry of the distributary channels changes the water-level variability of the whole region in calm conditions, as explained hereinafter. This approach is suggested to be used for simulating the dynamics of an extended domain of the region in the future works.

As explained in Section 3.4, The DTM is calibrated using different uniform Manning's coefficients. The effect of Manning's coefficient on all the modified DTMs follows the same trend: generally, high-tide water levels do not change considerably while low tide ones decrease with lower values of Manning's coefficient. This effect is favorable for some stations, but not for the others. For instance, lower (higher) roughness values lead to underestimation (overestimation) of low-tide water level along the WLO (in the floodplain). Consequently, among the values of n $= 0.018$, 0.02, 0.022, and 0.025 $s/m^{1/3}$, $n = 0.02\ s/m^{1/3}$ is chosen as the best compromise to be used for studying the effects of the width and depth of the distributaries.

Although these modifications mostly change the DTM of the distributaries in the forested floodplain area (refer to section 3.3 about the names of each area chosen in this study) and not in the Wax Lake delta and main channel, the dynamics of the whole region is affected by those changes. However, the way each station is influenced is different.

The results in the stations located in the main channel and delta are mostly dependent on the discharge capacity of the floodplain rather than solely on width and depth of the distributary channels. We found that changing either width or depth of the distributary channels while keeping their cross-sectional area almost constant has the same effect on the hydrodynamic of the Wax Lake outlet, meaning that one of the dominant parameters in the floodplain affecting the main channel is the wetted cross-sectional area of the distributary channels. For example, in Fig. 5a, the sensitivity of the station WL5 (as a representative of the stations located along the Wax Lake outlet) to the modification of the bathymetry is presented. During high tide, the sensitivity of the results to DTM modification is small, and all the cases underestimate the water level resulting from tidal flooding. This vertical shift of the model signals compared to the measured ones is related to low roughness coefficient used in WLO (which is corrected in Section 4.2). Focusing on the low-tide periods (because the model is most sensitive to the low-tide water level), it is observed that the results corresponding to narrow 1.5 m deeper and wide 1 m deeper (solid-red and dashed-green signals in Fig. 5a) are very close (Fig. 5a). Moreover, the overall pattern is that the higher the discharge capacity of the distributary channels, the higher the tidal damping (i.e., lower high water-level and higher low water-level). This may be due to the balance between frictional damping and topographic convergence (Jay, 1991). Increasing the discharge capacity of the distributary channels enhances the overall friction in the domain (because more water flows into the shallow distributaries). On the other hand, decrease of the discharge capacity leads to lower overall friction because water is driven to flow mainly in the deeper channels (increase of the system convergence in terms of overall wetted geometry), causing the amplitude of water-level signal to increase. This is why narrow 1 m deeper channels have the highest amplitude while the wide 2.5 m deeper channels have the lowest one. The balance between friction and convergence is a key factor in the tidal properties in each WL station; however, it is not straightforward for the CRMS stations probably due to the effects of other factors such as distributary connectivity.

The sensitivity of the CRMS stations to the DTM change is different from one station to the other (Fig. 5 and Appendix). Fig. 5b–d shows three of these behaviors: best results over the CRMS0464 station were obtained for narrow channel dug 1.5 m (dashed-green signal in Fig. 5b), but the sensitivity of the results become negligible with deeper and/or wider distributaries. This behavior may be due to the effects of the discharge capacity of its nearby lake (i.e., *Belle Isle Lake*). On the other hand, the water level at CRMS4016 is mostly dependent on the depth rather than width (in Fig. 8c, compare the solid and dashed lines of the same color, especially the ones in red). The reason is probably due to the fact that it is located along the bank of one of the main distributaries on the eastern side of WLO (between *Myrtle Bayou* and *Coalboat Pass*) and changing the width of the distributaries does not change its connection to the water flow in the region.

Station CRMS4808, located in the forested area on the western side of the Wax Lake outlet, has a smaller discharge capacity resulting in larger tidal dampening (with more significant changes at the low tides). It is not straightforward to choose the best case to simulate the ebb-tide periods in this station probably due to the high uncertainty of the bathymetry (especially the distributary bed profile) in its surrounding region. For the high-tide water levels lower than about 0.5 m (not shown in the main text, see Appendix), the model well follows the measurement. Interestingly, at two of the highest high-tide periods during which water level becomes higher than about 0.5 m, all the cases except the narrow-1m deeper case (dashed-red signal in Fig. 8d) fail to predict the water-level dampening observed in reality. This may indicate that different mechanisms become dominant in high-energy periods. This

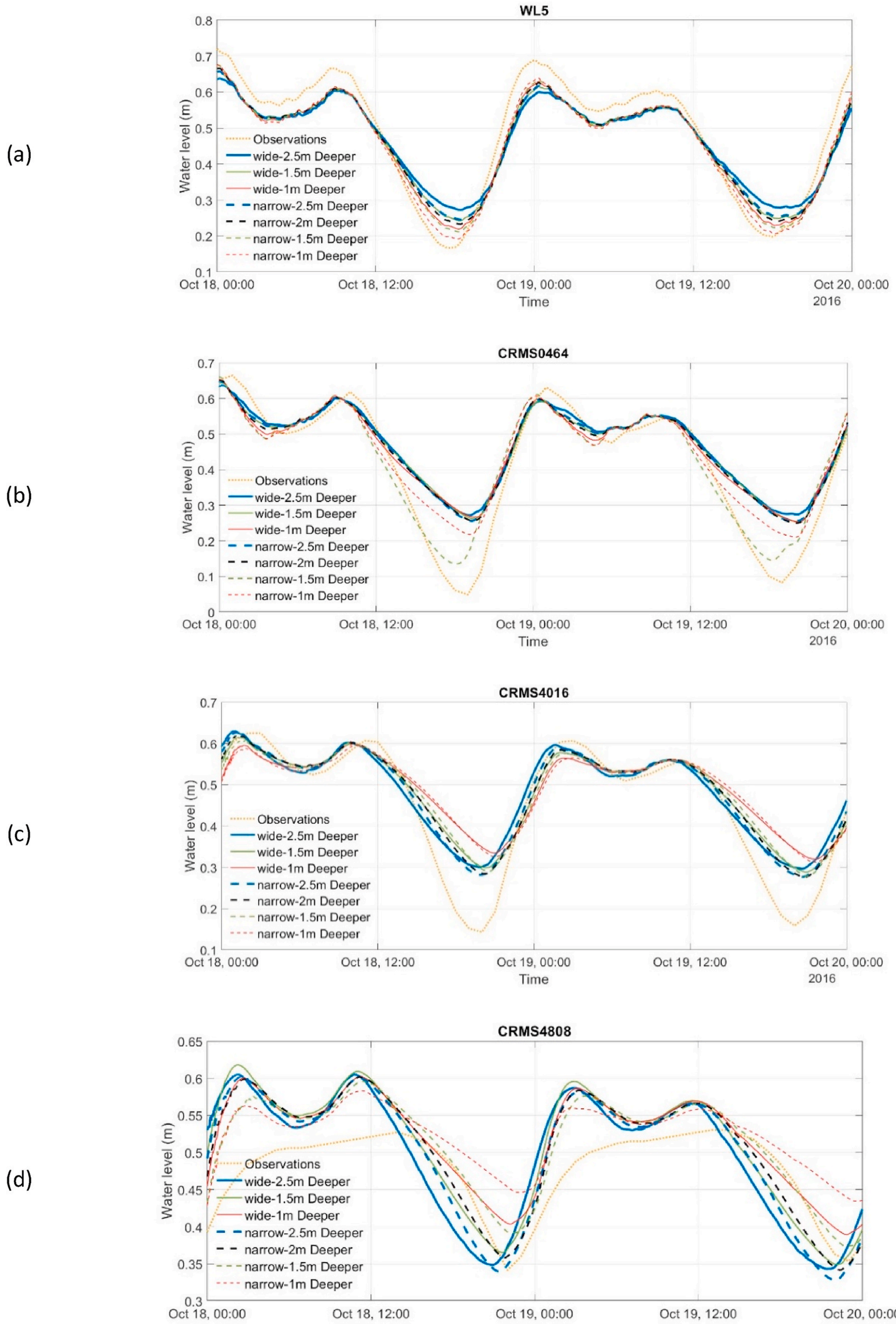

Fig. 5. Comparison and evaluation of the modelled water level time-series in four representative stations (with different behaviors) obtained using the modified DTMs.

behavior only occurs in the presence of vegetation. This area is covered mostly by herbaceous plants such as Colocasia esculenta (especially surrounding CRMS4809) and Nelumbo lutea (Daniel Jensen, JPL NASA, personal communication, 2018). These plants have a narrow stem with large leaves starting from about 1.5 m above the ground (Okonkwo, 1993) which may increase in their corresponding drag coefficient when water reaches a specific height. For the purpose of this study, we choose to ignore these effects of vegetation because they happen only in two high-tide periods of two of the stations.

In addition, the changes in the DTM causes a slight phase shift in the water-level signal in some of the CRMS stations. This may be due to the decrease of tidal wave celerity which is a function of water depth and friction (Cai et al., 2012). As a complementary to Figs. 5 and 6 statistically compares the efficiency of each modified DTM in WL1-WL9 and CRMS stations.

Considering the analyses explained in this section and the RMSE and R^2 values, the narrow 1.5-m-depth-correction DTM (explained in section 3.2.1) is chosen to have the best overall results for all of the measurement stations. This DTM will be used in the next stage to further improvement of the model including using spatially-variable bottom-roughness Manning's coefficient and (see Section 4.2).

Using the narrow 1.5-m-depth-correction DTM, Fig. 7 shows the water-level map at three different instances of the tide, i.e., low tide in the WLO (left), high tide in the WLO (center), and high tide in the floodplain (right). The time-series plot shown at the bottom of this figure corresponds to the water elevation at the ocean boundary. This figure illustrates the delay between the highest water level in the main channels and the one in the floodplain.

As mentioned earlier, it is assumed that overestimation of the low-tide water level (especially in the forested region) is due to the excessive flow resistance due to the uneven bed level along the distributaries. Following an iterative approach and upon using spatially variable Manning's coefficient (explained in the next section), this assumption is tested by manually changing the depth of all the computational cells

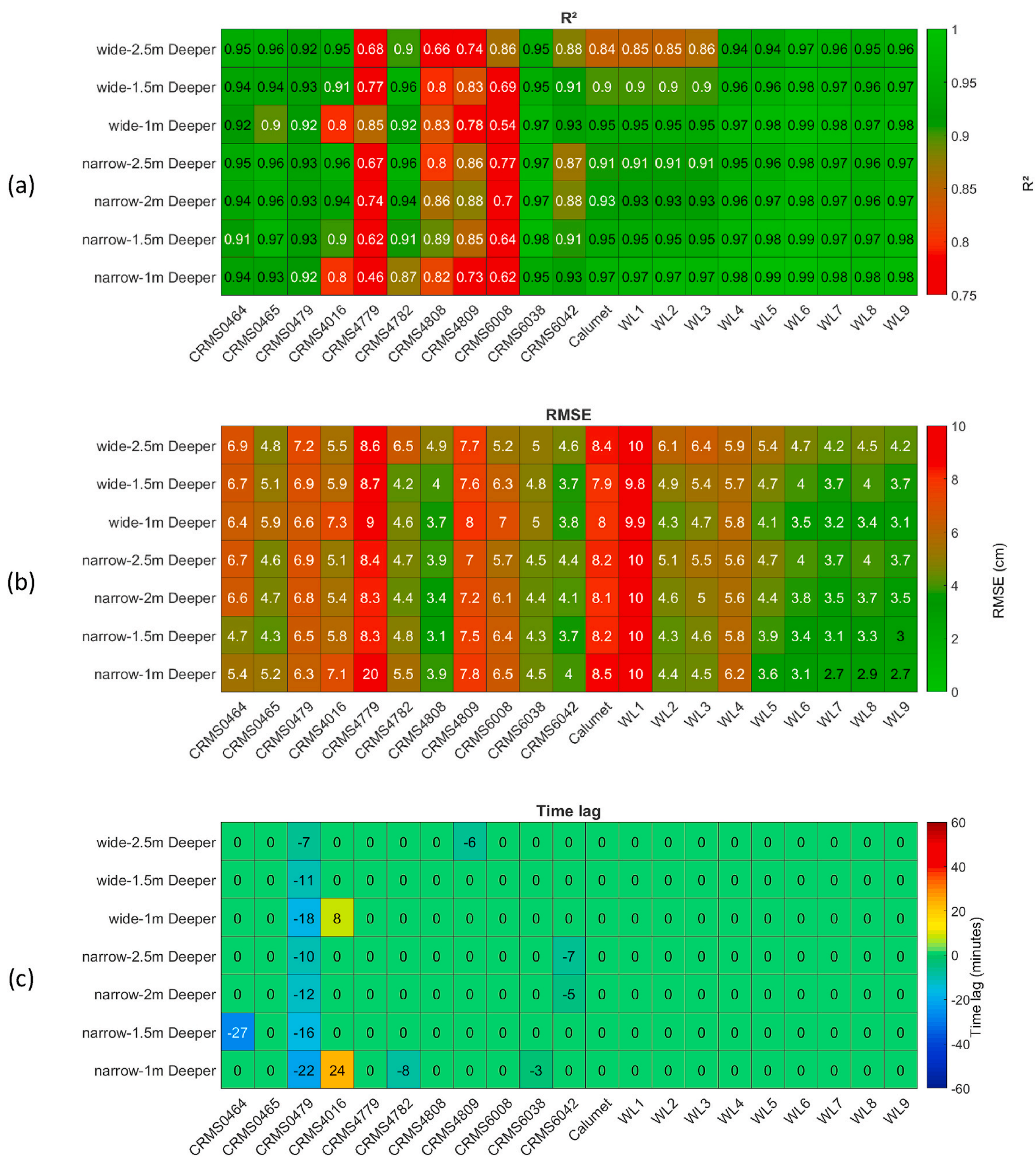

Fig. 6. Comparison of averaged R^2, RMSE and phase lag values for choosing the best version of DTM modification.

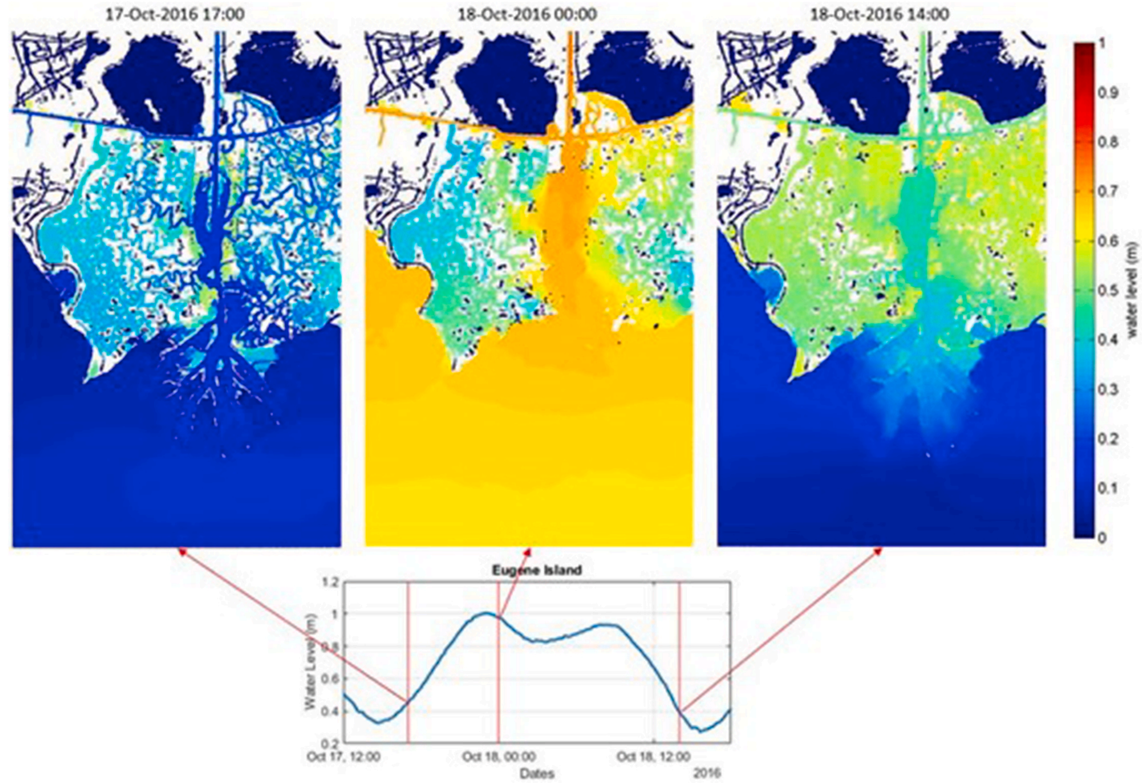

Fig. 7. Simulated flood map of the whole numerical domain at three instants. Left-hand-side map: at low tide in the Wax Lake Outlet. Middle map: at high tide in the Wax lake Outlet. Right-hand-side map: high tide in the floodplain.

which are between 1 and 2 m deep to 1.5 m deep. The resultant decrease in low water level is significant; for example, the drop at one of the low-tides is 7 cm and 4 cm for CRMS4808 and CRMS6008 respectively. In general, however, the results become better for some of the stations such as CRMS6008, but worse for some others (e.g., CRMS4808 especially because of increase in phase lag). This observation confirms that the bed of the distributaries may be flatter in reality than in the DTM and this difference leads to an overestimation of water level at a few stations during low tide. Moreover, it also indicates the increasing the resolution of the grid may not necessarily improve the results since larger grids intrinsically decreases the bed elevation change along the distributaries.

4.2. Further improvement of the model

In this section, the best model chosen from the previous section (i.e., narrow 1.5 m depth correction DTM) is used to test the effects of spatially-variable bottom roughness and vegetation in the model. Consequently, the effect of the WLO bottom roughness is examined and the vertical shift of water-level signal in some of the WL stations is corrected. Additionally, our tests confirm that ignoring the vegetation effects has been a reasonable assumption in this specific investigation.

For Wax Lake Outlet, higher Manning's roughness coefficient n is used to compensate the decrease of bottom roughness due to increase of depth (for example, Chow (1959) suggested the Manning's coefficient of $n = 0.03\ s/m^{1/3}$ for clean, straight, full stage, no rifts or deep pools). Two values of Manning's coefficient are considered for the WLO: one for the deeper section which is located from the upstream of WLO down to its cross-section with ICWW, and another for the rest of the river to WLD (Fig. 1c). As a result of this, the upstream water-level signal is shifted upward, especially in WL1, Calumet and CRMS4782 stations (this shift is also observed in WL3, CRMS6042, and CRMS6038, but the further southward stations are less affected); For the results not shown in Fig. 8, see Appendix. Consistently, the changes of the results in the delta are not remarkable. On the other hand, higher Manning's roughness coefficient (*n*) in WLO increases both the high- and low-tide water levels in the floodplain (with lower sensitivity in the high tide periods); therefore, n must be increased carefully. Furthermore, for the Wax Lake floodplain, low values of Manning's coefficient are used to decrease the water level during the low tides. Finally, the Manning's coefficient values provided in Table 1 are chosen to obtain the results shown in Fig. 8 and Appendix.

In Fig. 8, the respective values of average RMSE, R^2 and lag are also provided for each station. In comparison to Fig. 5, in general, the high tides in the WL stations and the low tides in both sets of observation points are slightly improved. Fig. 8 shows the result of WL3 as a representative station of the ones along the Wax Lake Outlet. In the delta, Manning's coefficient is $n = 0.018\ s/m^{1/3}$ in the main fan-shaped channels, and near the river bank, they are either 0.016, 0.014 or 0.012 (depending on their respective depth). The respective modelled water-level matches well with the measurement. Interestingly, comparing the results of WL6 and CRMS0479 (which are very close to each other and their main difference is that CRMS0479 is not in the main Wax Lake Delta channels but a small distributary) shows that a small distributary can have a remarkable effect on the results (i.e., here creates a phase lag and prevents the station to be drained enough).

Furthermore, as stated in Section 3.4, to examine the effects of vegetation, Baptist 2 formulation is used in this 2-D model. It resulted in damping the tidal energy, i.e., decreasing the high tide and increasing the low tide (Rodríguez et al., 2017) throughout the simulation which increases the error of the model. This trend is compatible with the long inundation time (known as "hydroperiod") observed at the two highest crests of the measured water-level signal in the observation stations CRMS4808 and CRMS4809 (during which the water level exceeds roughly 0.5 m, see Appendix). During these two periods, water becomes almost stagnant with a residence time of roughly 14 h, which is suggested it may be due to the effects of vegetation.

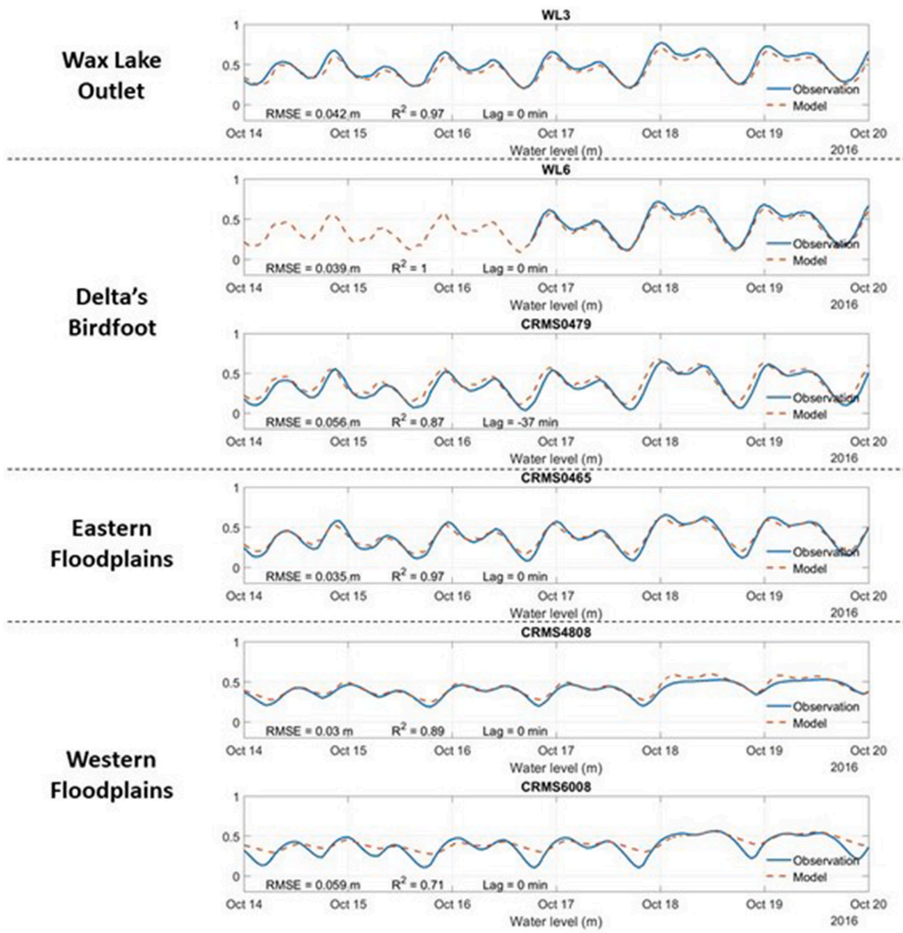

Fig. 8. Evaluation of the calibrated modelled water level time-series in some of the selected measurement stations.

Table 1
Manning's coefficients selected according to depth of the computational cells.

Depth threshold	22 < d	22 < d < 10	3 < d < 10	2 < d < 3	1 < d < 2	0 < d < 1	d < 0
Manning's coefficient [s/m$^{1/3}$]	0.06	0.035	0.018	0.016	0.014	0.012	0.02

5. Conclusions

WLO is a man-made channel with a large floodplain area containing a complex network of distributary channels. This region is relatively flat with a complex intertidal area, making it a suitable study zone to test the remote-sensing and hydrodynamic models in detecting/predicting the tide-induced surface water level change. This study simulates the flood-map evolution of WLO, delta and floodplain during the time period of October 14th, 2016 at 00:00:00 UTC to October 20th, 2016 at 00:00:00 UTC under three forcing of tide, river discharge and wind. Modeling results were evaluated by two sets of measurement stations to cover both river and floodplain tidal hydrodynamics.

This paper followed a novel approach to tackle the difficulties encountered due to lack of accurate bathymetric data for modeling a tidal-fluvial flat region. It was necessary to modify the original remotely-sensed DTM in order to better represent the distributary channels and thus obtain satisfying results over the floodplain in calm conditions. This task was accomplished by digging distributary channels in the floodplain, following Google Maps' water mask (Google, n.d.).

This study aims to provide the data to be used in calibration/validation phase of the SWOT mission. We have successfully calibrated the bathymetry to obtain a reasonably accurate hourly flood-map evolution of the region during one week. Both the grid spatial resolution (i.e., 46 × 45 m^2) and the model accuracy are well in the range required by SWOT (i.e., 100 × 100 m^2 and 10 cm respectively). The final bathymetry resulting to these data was selected following a sensitivity analysis of the model to the depth and width of the distributaries. Then, the effects of spatially-variable bottom roughness and vegetation were tested.

This investigation provides a useful methodology to calibrate the distributaries in a relatively flat intertidal area with a complex network of distributaries; it could be especially useful for future and more extended studies on this region. The model and calibration approach provides a useful tool to understand how the bathymetry and bottom roughness of the distributary channels and WLO bottom roughness contribute to the hydrodynamic of the region.

The effect of the width and depth of the distributaries on WLO is related to the discharge capacity of the floodplain. Increasing the discharge capacity of the distributaries results in lower water-level amplitude in the WLO because it means spreading more water in the secondary (shallow) channels relative to the main (deep) channel, thereby increasing of the overall wetted area and roughness. Accordingly, decreasing the discharge capacity brings the water mass towards the Wax Lake outlet, thereby decreasing the overall roughness and increasing the water-level amplitude. On the other hand, in the distributary network of the WLO flood plain, the improvement of the results with changing the DTM varies in different stations and in high- and low-tide periods. It is suggested that the different behavior mainly depend on the position of each station with respect to the main distributaries and ponds, the network of shallow distributaries, and/or vicinity to forested area. The results suggest that the stations located by the main distributaries mainly depend on the depth rather than width and connectivity. However, the stations within the network of shallow distributaries mainly depend on the discharge capacity of the channel cross-section of the distributaries.

In general, the calibrated model follows the observed-water-level changes well in the WLO while the main discrepancies occur in the floodplain. Additional tests suggest that flattening the bottom profile along the distributaries improves the results in the floodplain during the low-tide periods. Moreover, adding the effects of vegetation dampens the tidal amplitude which is an increase of the error in majority of the stations (the measurement shows this dampening effect only in two of the stations during two of their highest high tides), suggesting that ignoring the effects of vegetation in this investigation is reasonable, but it may not be the case for more energetic periods.

CRediT authorship contribution statement

Hassan Shafiei: Data curation, Formal analysis, Writing – review & editing, Validation, Writing – original draft, Software. **Antoine Soloy:** Conceptualization, Data curation, Formal analysis, Investigation, Validation, Methodology, Visualization, Writing – original draft, Writing – review & editing. **Imen Turki:** Supervision, Resources, Project administration, Funding acquisition, Conceptualization. **Marc Simard:** Conceptualization, Funding acquisition, Methodology, Project administration, Resources, Supervision. **Nicolas Lecoq:** Supervision, Project administration, Funding acquisition. **Benoit Laignel:** Funding acquisition, Project administration, Supervision.

Declaration of competing interest

The authors declare that they have no known competing financial interests or personal relationships that could have appeared to influence the work reported in this paper.

Acknowledgements

The authors are grateful to the COTEST international project funded by CNES-TOSCA, related to the future space mission called Surface Water and Ocean Topography (SWOT).

This work was partly performed by the Jet Propulsion Laboratory, California Institute of Technology, under contract with the National Aeronautics and Space Administration (NASA). Simard was funded within the framework of the SWOT Science Team, funded by NASA's Physical Oceanography Program.

The authors also acknowledge USGS, NOAA, and Google for providing the data used for this study including elevation, discharge, water level, and water mask data respectively.

Appendix A. Supplementary data

Supplementary data to this article can be found online at https://doi.org/10.1016/j.ecss.2021.107694.

Appendix

Comparison of the modelled and measured water-level signals obtained by the calibrated DTM including all the studied stations (An extended version of Fig. 8).

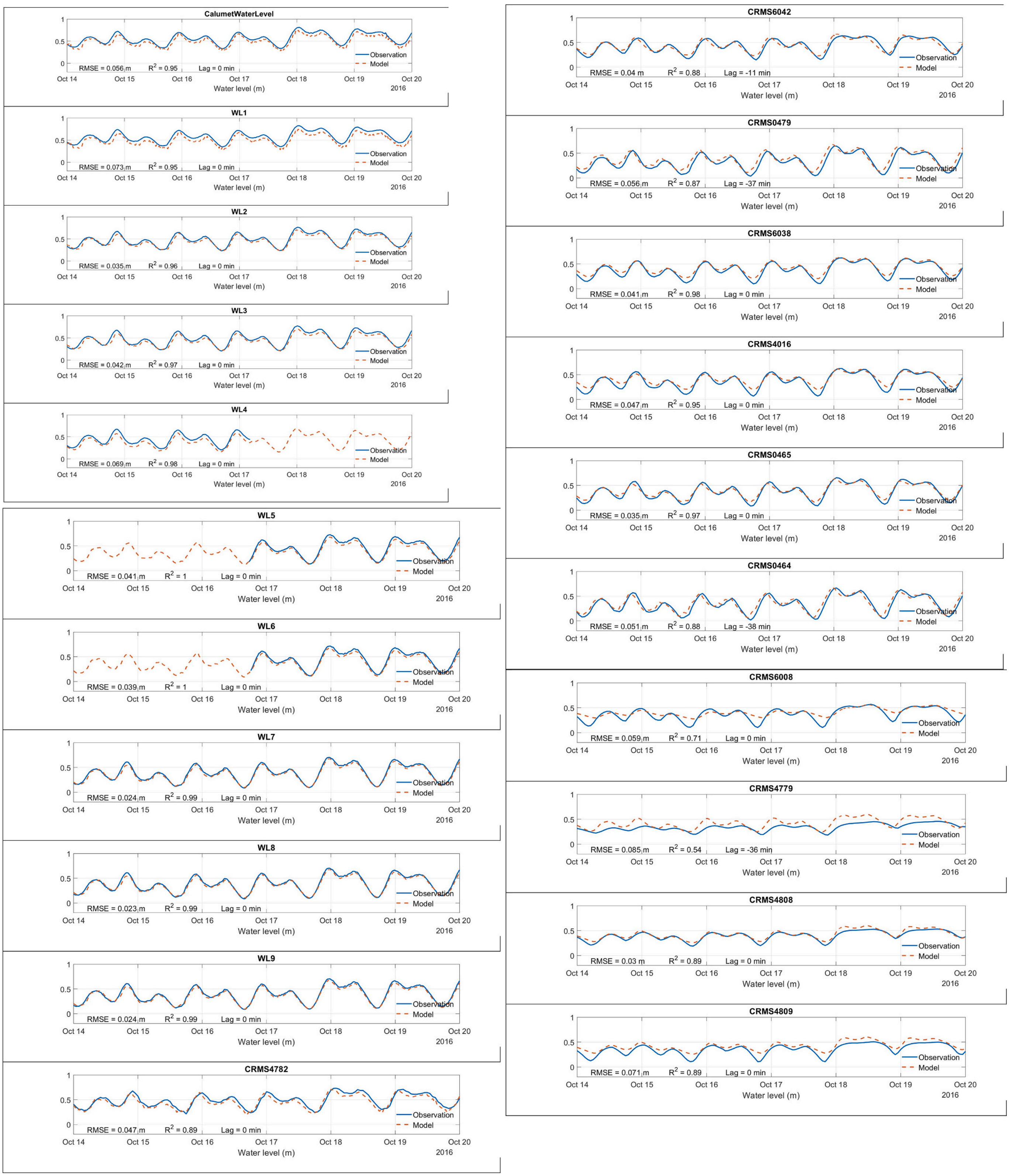

References

Al-Asadi, K., Duan, J.G., 2017. Assessing methods for estimating roughness coefficient in a vegetated marsh area using Delft3D. J. Hydroinf. 19 (5), 766–783.

Baptist, M.J., Babovic, V., Rodríguez Uthurburu, J., Keijzer, M., Uittenbogaard, R.E., Mynett, A., Verwey, A., 2007. On inducing equations for vegetation resistance. J. Hydraul. Res. 45 (4), 435–450.

Barbier, E.B., Georgiou, I.Y., Enchelmeyer, B., Reed, D.J., 2013. The value of wetlands in protecting southeast Louisiana from Hurricane storm surges. PLoS One 8 (3), e58715. https://doi.org/10.1371/journal.pone.0058715.
Buschman, F.A., Hoitink, A.J.F., Van Der Vegt, M., Hoekstra, P., 2010. Subtidal flow division at a shallow tidal junction. Water Resour. Res. 46 (12).
Cai, H., Savenije, H.H.G., Yang, Q., Ou, S., Lei, Y., 2012. Influence of river discharge and dredging on tidal wave propagation: modaomen Estuary case. J. Hydraul. Eng. 138 (10), 885–896.
Carle, M.M., 2013. Spatial Structure and Dynamics of the Plant Communities in a Prograding River Delta: Wax Lake Delta, Atchafalaya Bay. Louisiana (December).
Chow, V. Te, 1959. Open-channel Hydraulics. McGraw-Hill.
Christensen, A., 2017. Hydrodynamic Modeling of Newly Emergent Coastal Deltaic Floodplains. Louisiana State University Master Thesis (Issue December).
Davidson, R.A., States, U., & Station, U. S. A. E. W. E., 1988. Wax Lake Outlet Control Structure, Louisiana: Hydraulic Model Investigation. Waterways Experiment Station, p. 15 [31] pages.
Deltares, 2014. Delft3D-FLOW user manual, 1-710.
Denbina, M., Simard, M., Rodriguez, E., Wu, X., Chen, A., Pavelsky, T., 2019. Mapping water surface elevation and slope in the Mississippi River Delta using the AirSWOT Ka-band interferometric synthetic aperture radar. Rem. Sens. 11 (23), 1–26. https://doi.org/10.3390/rs11232739.
Denbina, M.W., Simard, M., Pavelsky, T.M., Christensen, A.I., Liu, K., Lyon, C., 2020. Pre-Delta-X: Channel Bathymetry of the Atchafalaya Basin. ORNL Distributed Active Archive Center, LA, USA. https://doi.org/10.3334/ORNLDAAC/1807, 2016.
Durand, M., Fu, L.-L., Lettenmaier, D.P., Alsdorf, D.E., Rodriguez, E., Esteban-Fernandez, D., 2010. The surface water and ocean topography mission: observing terrestrial surface water and oceanic submesoscale eddies. Proc. IEEE 98 (5), 766–779.
Edmonds, D.A., Slingerland, R.L., 2007. Mechanics of river mouth bar formation: implications for the morphodynamics of delta distributary networks. J. Geophys. Res.: Earth Surface 112 (F2).
Gaultier, L., Ubelmann, C., Fu, L.-L., 2010. SWOT Simulator Documentation. In: Rapp. Tech. JPL. NASA.
Gerritsen, H., de Goede, E.D., Platzek, F.W., van Kester, J.A.T.M., Genseberger, M., Uittenbogaard, R.E., 2008. Validation Document Delft3D- FLOW Validation Document Delft3D-FLOW. Deltares, pp. 1–182.
Gesch, D.B., Evans, G.A., Oimoen, M.J., Arundel, S.T., 2002. The national elevation Dataset. In: Digital Elevation Model Technologies and Applications: the DEM Users Manual, pp. 5–32. Issue 68.
Gomez-Navarro, L., Fablet, R., Mason, E., Pascual, A., Mourre, B., Cosme, E., Le Sommer, J., 2018. SWOT spatial scales in the western Mediterranean sea derived from pseudo-observations and an Ad Hoc filtering. Rem. Sens. 10 (4), 599.
Zhang, Y., Li, W., Sun, G., Miao, G., Noormets, A., Emanuel, R., King, J.S., 2018. Understanding coastal wetland hydrology with a new regional-scale, process-based hydrological model. Hydrological Processes 32 (20), 3158–3173. https://doi.org/10.1002/hyp.13247.
Google. (n.d.). Google Maps.
Gross, T.F., Werner, F.E., 1994. Residual circulations due to bottom roughness variability under tidal flows. J. Phys. Oceanogr. 24 (7), 1494–1502.
Hanegan, K.C., 2011. Modeling the Evolution of the Wax Lake Delta in Atchafalaya Bay. Louisiana.
Hiatt, M.R., 2013. A Network-Based Analysis of River Delta Surface Hydrology: an Example from Wax Lake Delta.
Hoitink, A.J.F., Jay, D.A., 2016. Tidal river dynamics: implications for deltas. Rev. Geophys. 54 (1), 240–272.
Horstman, E.M., Bryan, K.R., Mullarney, J.C., Pilditch, C.A., Eager, C.A., 2018. Are flow-vegetation interactions well represented by mimics? A case study of mangrove pneumatophores. Adv. Water Resour. 111, 360–371.
Horstman, E.M., Dohmen-Janssen, C.M., Narra, P.M.F., Van den Berg, N.J.F., Siemerink, M., Hulscher, S.J.M.H., 2014. Wave attenuation in mangroves: a quantitative approach to field observations. Coast Eng. 94, 47–62.
Hu, K., Chen, Q., Wang, H., 2015. A numerical study of vegetation impact on reducing storm surge by wetlands in a semi-enclosed estuary. Coast Eng. 95, 66–76.
Jay, D.A., 1991. Green's law revisited: tidal long-wave propagation in channels with strong topography. J. Geophys. Res.: Oceans 96 (C11), 20585–20598.
Jay, D.A., Borde, A.B., Diefenderfer, H.L., 2016. Tidal-fluvial and estuarine processes in the Lower Columbia River: II. Water level models, floodplain wetland inundation, and system zones. Estuar. Coast 39 (5), 1299–1324.
Jay, D.A., Leffler, K., Diefenderfer, H.L., Borde, A.B., 2015. Tidal-fluvial and estuarine processes in the lower columbia river: I. Along-channel water level variations, Pacific Ocean To Bonneville dam. Estuar. Coast 38 (2), 415–433.
Jung, H.C., Jasinski, M.F., 2015. Sensitivity of a floodplain hydrodynamic model to satellite-based DEM scale and accuracy: case study—the Atchafalaya Basin. Rem. Sens. 7 (6), 7938–7958.
Kathiresan, K., Rajendran, N., 2005. Coastal mangrove forests mitigated tsunami. Estuar. Coast Shelf Sci. 65 (3), 601–606.
Kim, W., Mohrig, D., Twilley, R., Paola, C., Parker, G., 2009. Is it feasible to build new land in the Mississippi River Delta? Eos. Trans. Am. Geophys. Union 90 (42), 373–374.
Leonardi, N., Kolker, A.S., Fagherazzi, S., 2015. Interplay between river discharge and tides in a delta distributary. Adv. Water Resour. 80, 69–78.
Lesser, G.R., Roelvink, J. A. v, Van Kester, J., Stelling, G.S., 2004. Development and validation of a three-dimensional morphological model. Coast Eng. 51 (8–9), 883–915.
Marsooli, R., Orton, P.M., Georgas, N., Blumberg, A.F., 2016. Three-dimensional hydrodynamic modeling of coastal flood mitigation by wetlands. Coast Eng. 111, 83–94.
Mcleod, E., Chmura, G.L., Bouillon, S., Salm, R., Björk, M., Duarte, C.M., Lovelock, C.E., Schlesinger, W.H., Silliman, B.R., 2011. A blueprint for blue carbon: toward an improved understanding of the role of vegetated coastal habitats in sequestering CO2. Front. Ecol. Environ. 9 (10), 552–560.
Megonigal, J.P., Neubauer, S.C., 2019. Biogeochemistry of tidal freshwater wetlands. In: Coastal Wetlands. Elsevier, pp. 641–683.
Nardin, W., Edmonds, D.A., Fagherazzi, S., 2016. Influence of vegetation on spatial patterns of sediment deposition in deltaic islands during flood. Adv. Water Resour. 93, 236–248.
Neeck, S.P., Lindstrom, E.J., Vaze, P.V., Fu, L.-L., 2012. Surface water and ocean topography (SWOT) mission. Sens. Sys. Next Gen. Satellites XVI 8533, 85330G.
Nicholls, R.J., Wong, P.P., Burkett, V., Codignotto, J., Hay, J., McLean, R., Ragoonaden, S., Woodroffe, C.D., Abuodha, P.A.O., Arblaster, J., 2007. Coastal Systems and Low-Lying Areas.
Okonkwo, C.A.C., 1993. Taro. In: Genetic Improvement of Vegetable Crops, pp. 709–715. https://doi.org/10.1016/b978-0-08-040826-2.50052-7.
Olliver, E.A., Edmonds, D.A., 2017. Defining the ecogeomorphic succession of land building for freshwater, intertidal wetlands in Wax Lake Delta, Louisiana. Estuar. Coast Shelf Sci. 196, 45–57. https://doi.org/10.1016/j.ecss.2017.06.009.
Osorio-Cano, J.D., Alcérreca-Huerta, J.C., Mariño-Tapia, I., Osorio, A.F., Acevedo-Ramírez, C., Enriquez, C., Costa, M., Pereira, P., Mendoza, E., Escudero, M., 2019. Effects of roughness loss on reef hydrodynamics and coastal protection: approaches in Latin America. Estuar. Coast 42 (7), 1742–1760.
Parker, G., Sequeiros, O., 2006. Large scale river morphodynamics: application to the Mississippi Delta. In: River Flow 2006: Proceedings of the International Conference on Fluvial Hydraulics, pp. 3–11.
Rivera-Monroy, V.H., Twilley, R.R., Davis III, S.E., Childers, D.L., Simard, M., Chambers, R., Jaffe, R., Boyer, J.N., Rudnick, D.T., Zhang, K., 2011. The role of the Everglades Mangrove Ecotone Region (EMER) in regulating nutrient cycling and wetland productivity in south Florida. Crit. Rev. Environ. Sci. Technol. 41 (S1), 633–669.
Rodríguez, J.F., Saco, P.M., Sandi, S., Saintilan, N., Riccardi, G., 2017. Potential increase in coastal wetland vulnerability to sea-level rise suggested by considering hydrodynamic attenuation effects. Nat. Commun. 8 (1), 1–12.
Roelvink, J.A., Van Banning, G., 1995. Design and development of DELFT3D and application to coastal morphodynamics. Oceanogr. Lit. Rev. 11 (42), 925.
Rouse Jr., L.J., Roberts, H.H., Cunningham, R.H.W., 1978. Satellite observation of the subaerial growth of the Atchafalaya Delta, Louisiana. Geology 6 (7), 405–408.
Sassi, M.G., Hoitink, A.J.F., de Brye, B., Vermeulen, B., Deleersnijder, E., 2011. Tidal impact on the division of river discharge over distributary channels in the Mahakam Delta. Ocean Dynam. 61 (12), 2211–2228.
Shaffer, G.P., Sassert, C.E., 2018. Published by. In: Shaffer, Gary P., Sasser, Charles E., Gosselink, James G., Rejmanek, Marcel (Eds.), Vegetation dynamics in the emerging Atchafalaya delta , Louisiana, vol. 80. British Ecological Society Stable, pp. 677–687. URL : https://www.jstor.org/stable/22608, 4.
Shaw, J.B., Mohrig, D., Wagner, R.W., 2016. Flow patterns and morphology of a prograding river delta. J. Geophys. Res.: Earth Surface 121 (2), 372–391.
Shields, M.R., Bianchi, T.S., Mohrig, D., Hutchings, J.A., Kenney, W.F., Kolker, A.S., Curtis, J.H., 2017. Carbon storage in the Mississippi River delta enhanced by environmental engineering. Nat. Geosci. 10 (11), 846–851.
Sievers, M., Brown, C.J., Tulloch, V.J.D., Pearson, R.M., Haig, J.A., Turschwell, M.P., Connolly, R.M., 2019. The role of vegetated coastal wetlands for marine megafauna conservation. Trends Ecol. Evol. 34 (9), 807–817.
Simard, M., Denbina, M.W., Jensen, D.J., Lane, R., 2020. Pre-Delta-X: Water Levels across Wax Lake Outlet, Atchafalaya Basin, LA, USA, 2016. ORNL DAAC, Oak Ridge, Tennessee, USA.
Simard, Marc, Denbina, M.W., Laignel, B., Liao, T.-H., Soloy, A., 2019. Remote sensing of the hydrological processes in the Mississippi river delta with the SWOT and delta-X missions. In: AGU Fall Meeting Abstracts, 2019, pp. OS23B–1785.
Stelling, G.S., Van Kester, J.A.T.M., 1994. On the approximation of horizontal gradients in sigma co-ordinates for bathymetry with steep bottom slopes. Int. J. Numer. Methods Fluid. 18 (10), 915–935.
Steyer, G.D., 2010. Coastwide reference monitoring system (CRMS). In: Fact Sheet. https://doi.org/10.3133/fs20103018.
Temmerman, S., Bouma, T.J., Van de Koppel, J., Van der Wal, D., De Vries, M.B., Herman, P.M.J., 2007. Vegetation causes channel erosion in a tidal landscape. Geology 35 (7), 631–634.
Thomas, N., Simard, M., Castañeda-Moya, E., Byrd, K., Windham-Myers, L., Bevington, A., Twilley, R.R., 2019. High-resolution mapping of biomass and distribution of marsh and forested wetlands in southeastern coastal Louisiana. Int. J. Appl. Earth Obs. Geoinf. 80, 257–267.
Whaling, A., Shaw, J., 2020. Changes to subaqueous delta bathymetry following a high river flow event, Wax lake delta, USA. Estuar. Coast 43, 1923–1938.
Xie, D., An, S., Davis, J.A., 2019. Preface: coastal wetlands: services, uses, and conservation. Hydrobiologia 827 (1), 1–2.
Xing, F., Kettner, A.J., Syvitski, J.P., Ye, Q., Bevington, A., Twilley, R., Atkinson, J.H., 2013. Impact of Vegetation on the Hydrodynamics and Morphological Changes of the Wax Lake Delta during Hurricanes. AGUFM, pp. EP13A–857.
Xing, Fei, Syvitski, J., Kettner, A., Meselhe, E., Atkinson, J., Khadka, A., 2017. Morphological responses of the Wax lake delta, Louisiana, to Hurricanes Rita. Elem Sci Anth 5.
Zhang, Q., 2015. Numerical Simulation of Cold Front-Related Hydrodynamics of Wax Lake Delta.